Well-ordered surface metal atoms complexation by deposition of Pd cyclometallated compounds on Ag (1 1 0)

Marija Stojkovska [a,b,1], Daniele Perilli [c,1], Jose Eduardo Barcelon [a,d], Marco Smerieri [a], Giovanni Carraro [a,e], Thuy Hien Dinh [b], Luca Vattuone [a,e], Mario Rocca [a,e], Gianangelo Bracco [a,e], Martina Dell'Angela [e], Roberto Costantini [e], Albano Cossaro [f,g], Luca Vaghi [c], Antonio Papagni [c], Cristiana Di Valentin [c,*], Letizia Savio [a,*]

[a] IMEM-CNR, UOS Genova, Via Dodecaneso 33, 16146 Genova, Italy
[b] Dipartimento di Chimica, Università degli Studi di Genova, Via Dodecaneso 31, 16146 Genova, Italy
[c] Dipartimento di Scienza dei Materiali, Università di Milano-Bicocca, Via R. Cozzi 55, 20125 Milano, Italy
[d] Dipartimento di Scienze Chimiche, della Vita e della Sostenibilità Ambientale, Università di Parma, Parco Area delle Scienze, 17/A, 43124 Parma, Italy
[e] Dipartimento di Fisica, Università degli Studi di Genova, Via Dodecaneso 33, 16146 Genova, Italy
[f] CNR-IOM, Strada Statale 14 – km 163.5, 34149 Trieste, Italy
[g] Dipartimento di Scienze Chimiche e Farmaceutiche, Università degli Studi di Trieste, via L. Giorgieri 1, 34127 Trieste, Italy

ARTICLE INFO

Keywords:
Pd cyclometallated compounds
Self-assembly
C-based networks
STM
DFT
Photoemission spectroscopy

ABSTRACT

In this paper we performed the deposition and self-assembly of a Pd-cyclometallated compound on Ag(1 1 0) surface for the first time. The system is investigated from the morphological and chemical point of view by scanning tunneling microscopy and x-ray photoemission spectroscopy, respectively, and the results are validated by ab-initio calculations. Our combined experimental and theoretical study aims at elucidating the atomistic details of the chemical steps following Pd cyclometallate deposition on the metallic substrate. To do that, we analyze the electronic and chemical properties of the species present on the surface at the end of the preparation process at room temperature and at 150 °C. We observe an unexpected complex chemistry: on one side, the organometallic molecules are found to dissociate into fragments, forming a well-ordered metal–carbon network; on the other side, Pd atoms become buried in the bulk of the metal substrate following metal exchange with surface Ag atoms. The details of this mechanistic study reveal the active role played by the metal substrate in promoting the chemistry of the deposited Pd cyclometallates and could open new perspectives for the application of this class of materials in heterogeneous catalysis.

1. Introduction

Among possible organometallic compounds, complexes of the Group 10 elements are attractive due to their widespread use in numerous applications such as catalytic synthetic processes [1–3], biological chemistry [4–6] and material science [7,8]. In particular, many palladium complexes have been extensively studied as catalysts in several cross-coupling reactions [9,10]. While great advancements have been made on the synthesis of transition metal (TM) complexes with specifically designed properties, our understanding about their interactions with metal surfaces is still quite limited. Their coupling to a surface is of interest, since their self-assembly on metal surfaces could lead to a major impact in catalysis and sensoristic. A fundamental requirement for such a strategy is the stability of the selected TM complex in the experimental conditions used for the surface deposition. Among the possible candidates, cyclometallated complexes display sufficiently high stability thanks to the presence of an E-M-C sequence of sigma bonds, where E is usually a group 15 or 16 donor atoms, M is a metallic center and C is a sp2 or sp3 carbon atom [11,12]. Up to now, for such compounds only few studies have been conducted for on-surface modification by using a bottom-up approach. For instance, Wilde et al. [13] successfully deposited Pt(II) cyclometallated on Ag(1 1 1) and demonstrated by STM that the intermolecular interactions upon 2D confinement are mainly driven by the entanglement of aliphatic side chains. Ren et al. [14]

* Corresponding authors.
E-mail addresses: cristiana.divalentin@unimib.it (C. Di Valentin), letizia.savio@imem.cnr.it (L. Savio).
[1] These authors contributed equally.

investigated the tetradentated Pt(II) complexes on various noble metal (1 1 1) surfaces and reported on the surface-mediated scission of the C-N bond in the organometallic compound upon annealing. They found out that the reactivity of the system strongly depends on the geometry of the coordination compounds and on the nature of the substrate. Similarly, dissociation of Ir(III) phosphorescent emitter molecules was observed on Cu(1 1 0) [15]. We note that all this work concerns cyclometallated complexes of the third-row transition-metal elements, such as Ir(III) and Pt(II), which are of interest as light emitters. To our knowledge, nothing has ever been reported on Pd cyclometallated complexes at metal surfaces, though these compounds are relevant especially for catalytic applications.

It is well-established that carbon-based nanostructures can be doped with hetero-atoms to tune their electronic and chemical properties [16]. By far, most of the experimental studies concern doping with non-metal atoms (e.g., N, P, S, B), reaching a good characterization of these systems. The next step is the introduction of TM atoms, since TM containing C-networks are predicted to have interesting electronic and catalytic properties. These new and low-cost materials could, in principle, replace currently used catalysts based on precious transition metals, so that interesting applications in sensoristic and nanocatalysis can be envisaged.

There are several ways to grow C-based nanostructures [17–21]. Self-assembly of suitable molecular precursors at metal surfaces, possibly followed by polymerization, was proven to guarantee the best degree of order and uniformity of the 1D or 2D C-based networks [22,23].

Doping with TM atoms was achieved by the reaction of suitable precursors on nanoporous carbon materials, which were then demonstrated to be efficient towards the oxygen oxidation reaction [24]. Similarly, Pd(II)-based 2D mesoporous covalent organic frameworks have been recently synthesized and successfully employed as eco-friendly heterogeneous photocatalysts for CO_2 cycloaddition [25]. Much less experimental information is available for supported 2D and 1D nanostructures. TM atoms could be inserted *a posteriori* once the C-layer has already been produced. However, due to their high surface energy, they can be unstable and cluster together. Alternatively, TM atoms can be introduced in the network during its formation using suitable organometallic precursors. In this case, stabilization of the TM is achieved via the presence of other non-metallic elements, such as nitrogen (e.g. by N-TM-C bonds). Theoretical models of such hybrid metal/non-metal/carbon networks suggest promising results, while the development of such systems and their understanding at the fundamental level (including a detailed characterization of their morphological, electronic, and chemical properties) is still lacking.

In this paper we report for the first time on the deposition of a Pd cyclometallated compound on a metal surface. We present an experimental and theoretical investigation of the interaction of [(5-bromo-2-phenylpyridine)Pd(μ-Cl)]$_2$ ($C_{22}H_{14}Br_2Cl_2N_2Pd_2$, **CyPd** in the following) with Ag(1 1 0). The choice of Ag(1 1 0) as a substrate is due to its intermediate reactivity among coinage metals. This often allows for intermolecular interaction to prevail over molecule-surface attraction, so that uniform and extended self-assemblies may form. The dinuclear Pd complex was chosen for its planar structure and its high thermal stability, besides bearing two metal atoms/molecule. The organic ligand was brominated, aiming at a surface-assisted organization, as we previously observed for bromoarenes [23,26]. Since, as mentioned before, there is no previous literature on this topic, we focused our attention on the stability of the compound upon adsorption and on the change in molecular conformation, with the aim of evaluating if the system can be suitable as a model for catalytic studies.

The **CyPd**/Ag(1 1 0) system is characterized upon deposition of the molecules at room temperature (RT) and subsequent annealing up to 150 °C by combining the morphological information provided by scanning tunnelling microscopy (STM) with the chemical one derived from X-ray photoemission spectroscopy (XPS) measurements. Based on density functional theory (DFT) calculations, we propose a reaction mechanism and an adsorption model, which are then validated by simulated STM images and by a Near Edge Adsorption Fine Structure (NEXAFS) analysis. Our results indicate a complex chemistry at the surface: the Ag surface promotes dissociation of **CyPd** in two phenylpyridine (phe-pyr) fragments. Each fragment is coordinated by an Ag adatom provided by the substrate, thus forming a network of organometallic compounds, while the Pd atoms migrate in the subsurface region. The dissociated halogen atoms are stabilized on the surface by Ag atoms. The final configuration is more complex than expected, suggesting an active role of the metal substrate. Our results give an in-depth understanding of the chemistry between metal surfaces and Pd cyclometallated complexes and elucidate the electronic and chemical properties of this class of materials.

2. Experimental and computational details

2.1. Synthesis

The Pd cyclometallate [(5-bromo-2-phenylpyridine)Pd(μ-Cl)]$_2$ (**CyPd** – see Fig. 1A1 for the molecular structure) was synthesized according to the procedure of Yian Shi and coworkers [27]. Thus, $PdCl_2$ was reacted with a slight excess (1:1.05) of 5-bromo-2-phenylpyridine in $CHCl_3$, at a temperature of 100 °C (sealed tube, inert atmosphere) for 24 h. The precipitate formed was recovered by filtration and washed extensively with $CHCl_3$ to afford **CyPd** in a pure form as highly insoluble yellow solid. Thermogravimetric analysis of **CyPd** showed high thermal stability since decomposition occurred above 320 °C (Figure S1 in the Supporting Material). Details of the synthesis and characterization of **CyPd** are presented in the Supporting Material (SM – Figures S1-S3).

2.2. Experimental methods

Surface science experiments were carried out in two different UHV chambers equipped for Low Temperature Scanning Tunneling Microscopy (LT-STM) and for High Resolution X-Ray Photoemission Spectroscopy (HR-XPS), respectively.

The former setup, present at the IMEM-DIFI laboratory in Genova, consists of a main chamber hosting the LT-STM (manufactured by Createc) and of a preparation chamber equipped with a homemade evaporator for deposition of organic molecules and with all typical vacuum facilities for sample cleaning and residual gas analysis.

STM images were recorded at liquid nitrogen (LN_2,77 K) or liquid helium (LHe, 4 k), using a Pt/Ir tip. The images were acquired in constant current mode, with typical tunneling currents $0.1nA \leq I \leq 0.8nA$ and a bias voltage range $-2.0\ V \leq V \leq +2.0\ V$ applied to the sample. Surface orientation and image dimensions were determined from atomically resolved images of clean Ag(1 1 0) as the one reported in Fig. 1A2; similarly heights were calibrated on monoatomic Ag steps. STM analysis was performed in WSxM software. [28].

Photoemission and NEXAFS experiments were carried out at ANCHOR-SUNDYN end-station of the ALOISA beamline at the Elettra synchrotron radiation facility (Trieste, Italy) [29], using a Phoibos 150 analyzer (SPECS manufacturer).

XPS spectra were recorded using a photon energy $h\nu = 515$ eV. The binding energies (E_b) were calibrated on the Fermi edge of the Ag(1 1 0) substrate, from which also an instrumental resolution of 0.15 eV could be determined. After calibration, the Ag $3d_{5/2}$ line of the clean surface sits at E_b(Ag $3d_{5/2}$) = 368.21 eV, in perfect agreement with literature data [30]. Core level spectra were fitted with Doniach-Sunjic line shapes convoluted with a Gaussian profile after subtracting a linear background. An error of ±5 % is estimated for the fitted intensities. Up to four components were necessary to reproduce the C 1s region, while only two were sufficient for the N 1s peak. Ag 3d, Pd 3d, Cl 2p and Br 3d regions were fitted with doublets considering the spin–orbit splitting.

The NEXAFS spectra were acquired in Auger electron yield mode

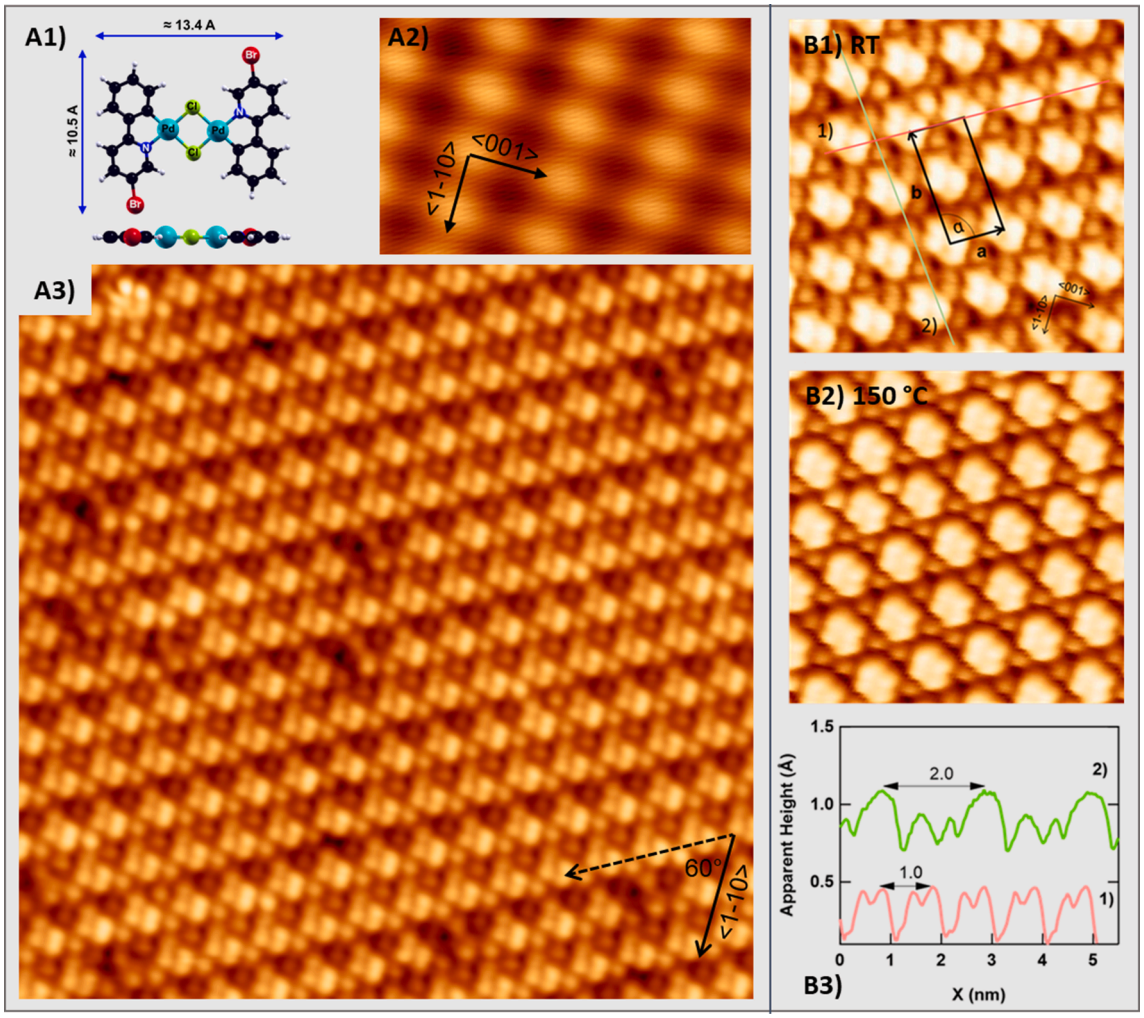

Fig. 1. Part A) – Deposition of CyPd on Ag(1 1 0). A1) Chemical structure of the Pd cyclometallate [(5-bromo-2-phenylpyridine)Pd(μ-Cl)]$_2$ (**CyPd**). A2) Atomically resolved image of clean Ag(1 1 0), on which the high symmetry directions are marked (black arrows). Image size: 2.0 × 1.3 nm^2, V = 0.06 V, I = 0.42 nA. A3) Overview STM image recorded after 30 min deposition of **CyPd** on Ag(1 1 0) at RT. Image size: 15x15 nm^2, V = -0.4 V, I = 0.64 nA, imaging at 4 K. **Part B) – Details of the self-assembly.** B1) High resolution STM image of the self-assembled layer in A3). The unit cell is marked by the black rectangle. The high symmetry directions of Ag(1 1 0) are marked in the bottom-right corner. B2) Same as B1) upon annealing to 150 °C for 5 min (Imaging at 80 K). In both cases, image size: 6 × 6 nm^2, V = −0.1 V, I = 0.1 nA. B3) Height profiles cut along the red and green traces in panel B1), corresponding to the unit cell directions **a** and **b**, respectively.

recording C and N KVV Auger electrons with the hemispherical electron analyzer fixed at a kinetic energy of 262 eV and 385 eV for the C and N K-edges, respectively. A two-step normalization process is used for the spectra: first, a multiplication factor is applied to scale the intensity before the energy threshold to the one of the clean surface, thus correcting for unwanted variations of the X-ray beam intensity; then the ratio between the so-normalized spectrum and the spectrum of the clean surface is plotted [31]. This second step reduces the signals due to impurities and substrate, leaving only the contributions of the adsorbates in the NEXAFS signal.

The Ag (1 1 0) surface was cleaned by cycles of sputtering with Ne (Ar) ions followed by annealing for 5 min to T = 537 °C (T = 570 °C) for microscopy (spectroscopy) experiments. **CyPd**, sublimated from a Ta crucible resistively heated to 130 °C, was deposited on Ag(1 1 0) at RT and step-annealed for 5 min to 100 °C and 150 °C, always keeping a background pressure better than 2.0 10^{-9} mbar. At each step, the morphology and thermal evolution of the self-assembled organometallic layer was monitored by STM while its chemical composition was checked by HR-XPS.

2.3. Computational details

Density Functional Theory (DFT) calculations were performed using the plane-wave-based Quantum ESPRESSO package (QE) [32–34]. The ultrasoft pseudopotentials were adopted to describe the electron–ion interaction with Ag (4d, 5s), Pd (4d, 5s), C (2s, 2p), N (2s, 2p), Cl (3s, 3p), Br (4s, 4p), and H (1s) treated as valence electrons. Energy cutoffs of 45 Ry and 360 Ry (for kinetic energy and charge density expansion, respectively) were adopted for all calculations. The Van der Waals density functional vdW-DF2^{C09x} was used for electron exchange–correlation [35], which gives an accurate description of the adsorption energies and distances of graphene on metal surfaces [36] and has also been successfully applied to describe self-assembly of brominated tetracene (DBT) on different metal surfaces [26,37–39].

For the simulation of the Ag(1 1 0)-supported **CyPd** (**CyPd**/Ag), a $(2\sqrt{3}\mathbf{a} \times 3\sqrt{3}\mathbf{b})$R55 supercell was used, where **a** and **b** are the lattice vectors of the Ag(1 1 0) unit cell (2.88 Å and 4.07 Å, respectively, in perfect agreement with the experimental values). Such a cell has been chosen to match the experimentally determined one (see Section 3).

The geometry relaxation of all considered systems was performed with a 4 × 2 × 1 Monkhorst-Pack k-points mesh [40], followed by a non-self-consistent field (NSCF) calculation with a 12 × 6 × 1 Monkhorst-

Pack k-points mesh for evaluating the electronic properties.

The Ag(1 1 0) surface was modeled by a three-layer slab with the bottom layer fixed to the bulk positions during the geometry relaxation to mimic a semi-infinite solid. To avoid interactions between adjacent periodic images, a vacuum space of about 25 Å in the direction perpendicular to the surface was used.

STM simulations were performed using the Tersoff-Hamann approach [41], according to which the tunneling current is proportional to the Energy-Integrated Local Density of States (ILDOS). STM images were rendered with Gwyddion software [42]. Constant-current and voltage values for the STM simulations were chosen to match the experimental values.

3. Results and discussion

3.1. Experimental section

Deposition of **CyPd** on Ag(1 1 0) at RT leads to the formation of extended self-assembled patterns as the one shown in the overview of Fig. 1A3. First of all, we mention that no isolated molecules are observed on the surface, while bare Ag(1 1 0) patches may coexist with fully covered areas depending on the total coverage achieved. On the other hand, no traces of multilayer have been observed in the present experimental conditions even after prolonged exposures. This indicates that **CyPd** adsorption is a self-limiting process: an attractive interaction among molecules is present and, at RT, they are mobile enough to diffuse on the surface to nucleate a new island of molecules or join an already existing one.

The 2D-network consists of lozenge-shaped features assembled in a double row-structure. The rows are oriented ±(60°±3°) off the < 1–10 > direction. Each feature consists of four lobes of slightly different brightness arranged in a rhomboidal shape and are surrounded by some interstitial dots. The enlarged image of Fig. 1B1 showcases these details.

Fig. 1B compares the morphology of the **CyPd**/Ag(1 1 0) sample as grown at RT and after annealing to 150 °C. No significant changes are observed in the layer upon annealing to T = 100 °C (not shown) and to 150 °C. Statistical analysis of several equivalent images and of line scans as the ones reported in panel B3 allowed us to determine the typical periodicities of the self-assembled geometry and to draw the unit cell marked in panel B1. At RT, it is nearly rectangular, with unit cell vectors a=(0.97 ± 0.04) nm and b=(2.01 ± 0.10) nm aligned along the rows and perpendicular to them, respectively. The unit cell parameters are compatible within the error for the sample as grown and after annealing (see Table S1 in the SM), confirming the intuitive indication that the observed self-assembled geometry is stable in the investigated temperature range. We mention that a smaller unit cell is not possible since the pairs of rows are slightly misaligned and the separation between one row and the next is not the same on either side.

Each unit cell contains two lozenge-shaped features and four smaller and fainter dots. By comparing the experimentally determined values of the unit cell with the expected molecular dimensions of the isolated **CyPd** molecule (1.34 nm long and 1.05 nm wide), we estimate a population of one molecule per unit cell, corresponding to a local coverage of $(5.1 \pm 0.1)\cdot 10^{13}$ molecules/cm^2. The two large features could thus correspond to the two halves of the molecule, while the nature of the dots is less straightforward. For analogy with previous literature on halogenated aromatic systems on the same surface [23,26], we can tentatively assign them to dissociated Br atoms and/or Ag adatoms taken from the substrate; however, this hypothesis needs to be verified due to the larger complexity of the **CyPd**/Ag(1 1 0) system. Moreover, we note that the structure of **CyPd** consists of two equivalent parts rotated by 180° with respect to each other, while careful inspection of the high-resolution images of Fig. 1B shows that all the lozenges have the same shape and orientation.

Further analysis with complementary tools is therefore necessary for a complete understanding of the system. The chemical information, which is absent in STM images, is provided by the high resolution XPS spectra of Figs. 2 and 3. The former shows the Br 3d (panel a) and C 1s (panel b) spectra recorded during an **CyPd** uptake on Ag(1 1 0) at RT. Incremental doses were performed until the saturation coverage was reached, corresponding to the completion of a full monolayer according to STM inspection. The total C 1s and Br 3d areas are reported in panel c. Fig. 3 shows, on the contrary, the N 1s, C 1s, Cl 2p and Br 3d regions for the full **CyPd** monolayer of Fig. 2 (bottom traces) and their evolution upon annealing to 150 °C (top traces). The outcome of the fitting procedure is also reported to evidence the different components contributing to each spectrum.

We first note that only one doublet is present in the Br 3d region at $E_b(Br\ 3d_{5/2}) = 68.1$ eV, i.e. at a binding energy corresponding to Br atoms bound to Ag. On the contrary, no traces of Br-C bonds appear around 70 eV [23,43]. This behavior is already evident at the smallest dose and it is indicative that full debromination of **CyPd** occurs on Ag (1 1 0) already at RT, coherent with what is observed for other halogenated aromatic hydrocarbon species [23,37,44]. The Cl 2p spectrum, characterized by a doublet with $E_b(Cl\ 2p_{3/2}) = 197.6$ eV, is less conclusive since this binding energy is suitable for Cl atoms bound either to Pd or Ag [45], so that it is not possible to determine from XPS spectra if Cl atoms remain bound to the molecule or if they dissociate upon adsorption.

The C 1s spectrum observed at RT has already a strongly asymmetric shape at the smallest coverage. It clearly reveals the presence of multiple components corresponding to C atoms in different chemical environments. The main line at $E_b = 284.7$ is assigned to the unresolved contributions of sp^2 C atoms (C—C component) and C—H bound carbon atoms [23,37]. The components at $E_b = 285.3$ eV and 286.0 eV are in the range suitable for C-N bonds [46].

The N 1s spectrum shows a single feature, which can be resolved into two components: a main one at 399.4 eV and minor one at 398.6 eV. According to previous literature [47], both species are suitable for pyridinic nitrogen, though their assignment is not straightforward. They could correspond to N atoms with a slightly different interaction with the Ag substrate. An E_b value corresponding to the higher energy component was observed for bi-isonicotinic acid on Ag(1 1 1) and attributed to nitrogen atoms weakly interacting with the substrate [48]; on the contrary, the lower energy component is compatible with the signal measured in N-doped graphene on Ni(1 1 1) [49] and may therefore indicate, in the present case, a stronger interaction with the substrate and possibly N—Ag bond formation. We mention that a very weak upshift of the Ag $3d_{5/2}$ line is observed reproducibly upon deposition of ~ 1 monolayer of CyPd (see Figure S4 in SM), suggesting that a small amount of Ag atoms may have formed chemical bonds with the adsorbate.

Heating up the sample to 150 °C causes desorption of the aromatic part of the molecule, as witnessed by a ~40 % decrease of the C 1s and N 1s intensity. In the C 1s region, we observe a small downshift of ~0.1 eV in E_b and the appearance of a small additional component at 283.4 eV, which may be either due to some segregation of C induced by the annealing process or by the formation on additional Ag-C bonds. In this case, they should be different from those already formed at RT upon debromination. In the N 1s region, on the contrary, the intensity ratio of the two components gets inverted. Therefore, the amount of N atoms interacting more strongly with Ag increases slightly though the overall coverage decreases with annealing. However, the change in the N 1s spectrum is not reflected in the geometry of the self-assembled overlayer, which remains the same except for minor changes in the internal structure of the lobes. Finally, annealing does not cause significant changes for Cl 2p and Br 3d regions, suggesting that the halogen atoms remain stable on the surface.

The last elemental constituent of the **CyPd** molecule is Pd. Though the presence of such element was checked in the XPS spectra, and though its cross section under the present experimental conditions should allow to see a measurable signal in the Pd 3d region, almost no

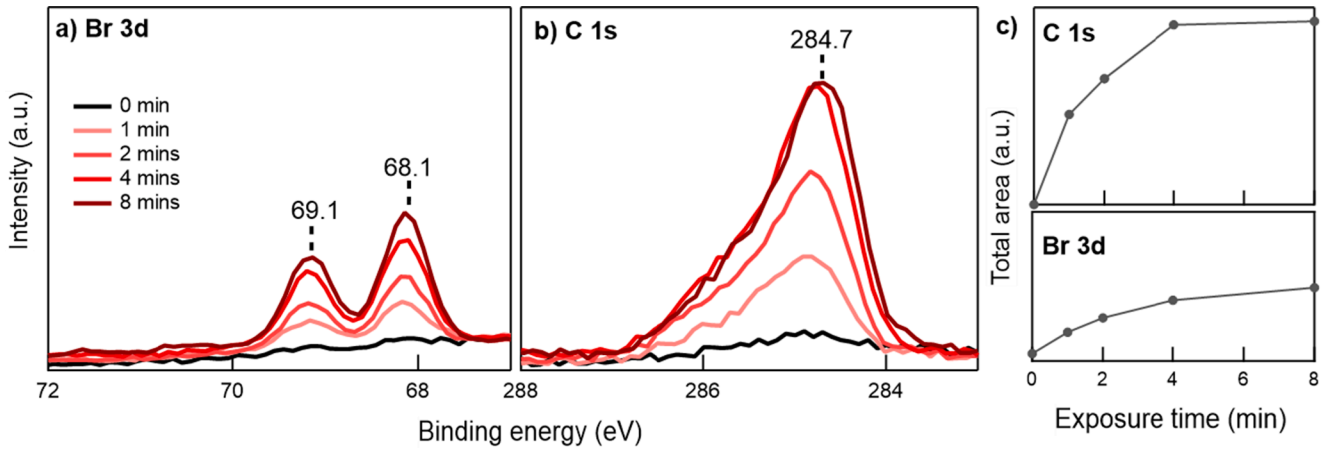

Fig. 2. XPS spectra of a) Br 3d and b) C 1s regions for the Ag(1 1 0) surface clean (black trace) and after increasing exposure of **CyPd** at RT (red traces). c) Total C 1s and Br 3d areas vs exposure time.

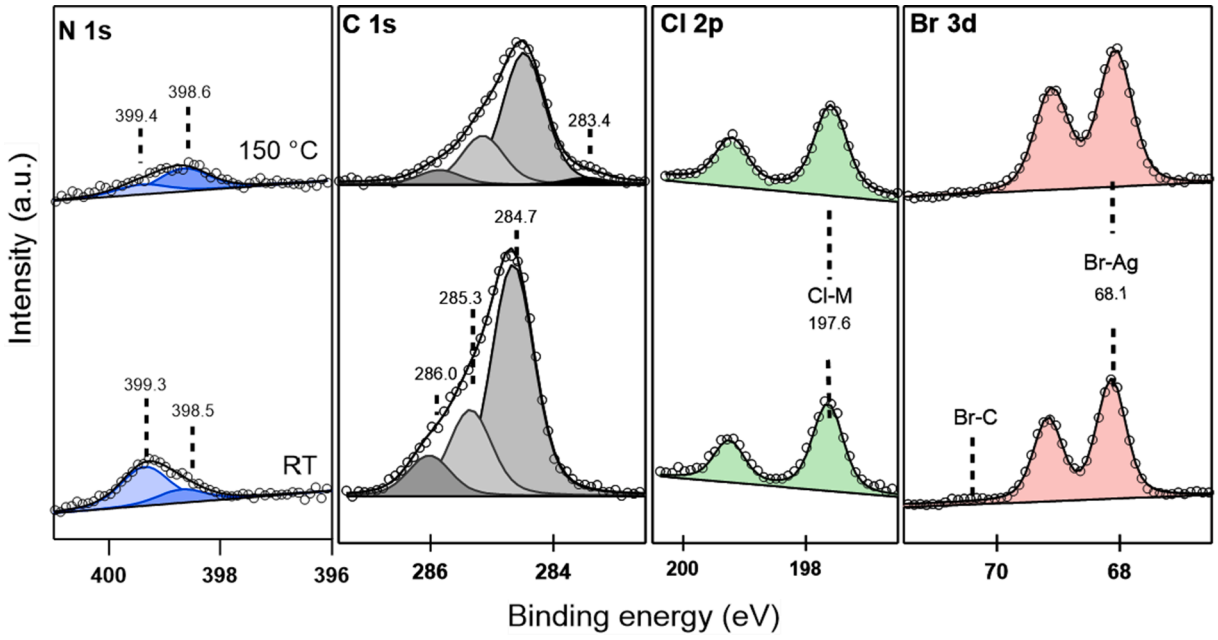

Fig. 3. XPS spectra of C 1s, N 1s, Cl 2p and Br 3d regions recorded for **CyPd**/Ag(1 1 0) at RT and saturation coverage and after 5 min step-annealing up to 150 °C (upshifted for sake of clarity). The outcome of the fitting procedure and the different components identified are reported in each region.

intensity was observed around 335 eV (Pd $3d_{5/2}$) (see Figure S5 in the SM). This indicates a final configuration in which the Pd atoms are efficiently screened, as discussed in the following. The possibility that the molecule dissociates in the crucible during sublimation is ruled out since: i) The stoichiometric ratio of the other elements is respected (see table S2 and relative discussion in SM) and the adsorbate organizes on the surface in an ordered, reproducible and periodic structure. If fragments were produced into the crucible, they would necessarily have different sublimation temperatures and hence their relative abundance on the surface should be far from molecular stoichiometry. ii) The ATR-FTIR and XPS analysis of the **CyPd** powders as prepared and after several sublimation cycles in the crucible yielded perfectly compatible results, indicating that no degradation of the molecule had occurred (see Figures S2 and S3in the SM).

3.2. Computational section

The Ag(1 1 0) supercell model that was considered in the computational study (purple full cell in Fig. 4a) is almost coincident with the experimentally determined repeating unit and it is characterized by a surface area sufficient to support one Pd dimer complex ($C_{22}H_{14}Br_2N_2Pd_2Cl_2$).

We started by depositing the undissociated molecule (Model 1 in the scheme of Fig. 4b). Though this choice is at variance with the experimental evidence provided by XPS, which indicates full debromination of the **CyPd** units already at RT, it is functional to our study. The optimized geometry for this configuration is reported in Fig. 5ab (Model 1a) together with the simulated STM image at V = −0.1 V. This situation is not the most advantageous from an energetic point of view (first line in Table S3) and the agreement with the experimental STM images reported in the previous section is quite poor. The bright features, one per unit cell, nicely reproduce the shape of the molecule; however, they are too large with respect to the experimental ones, which indeed are too small to represent one entire molecule each. Therefore, as a next step, we removed both Br atoms from the molecule (Model 1b in Figure S6); unfortunately, this does not significantly improve the situation and the appearance of the molecular feature.

Experimentally, in each supercell unit we observe two bright spots of

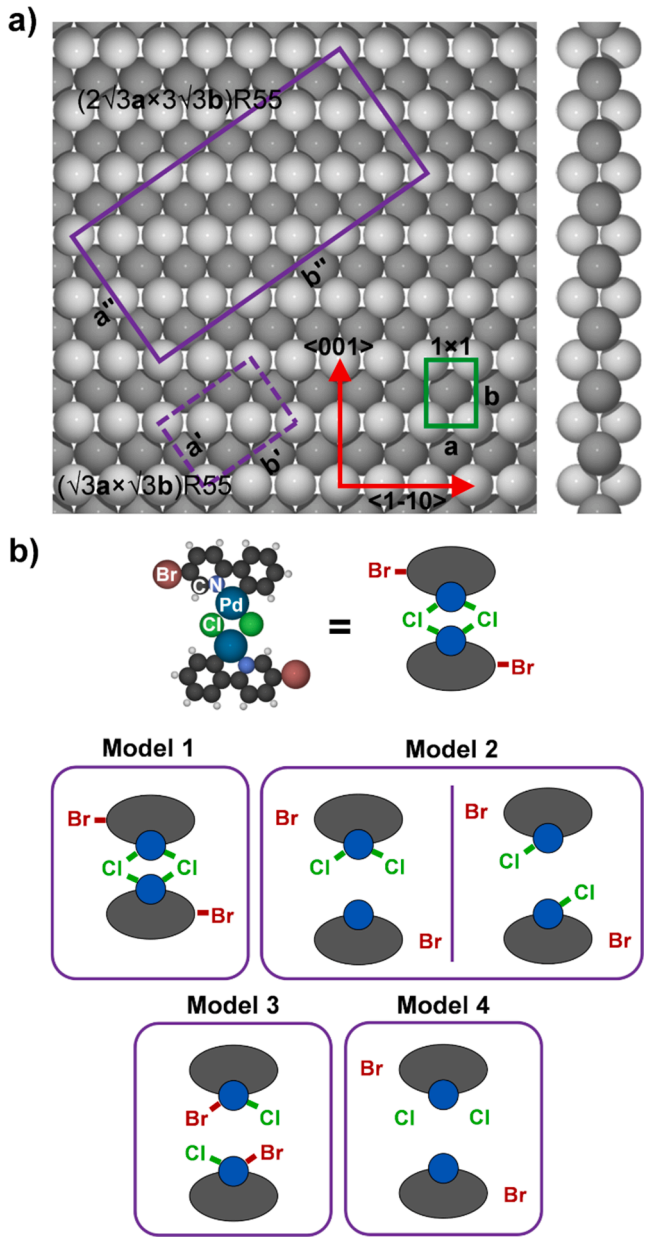

Fig. 4. a) Top and side view of Ag(1 1 0). The surface unit cell is shown in green, whereas the smallest unit cell with the same orientation as the experimental one (rotated by ≈60° with respect to the ⟨1–1 0⟩ direction) is marked in dashed purple. Given the size of **CyPd**, a (2 × 3) supercell was used (purple full cell). Ag atoms in the top and bottom layer are rendered in light grey; Ag atoms in the middle layer are rendered in dark grey. b) Scheme of possible adsorption/dissociation configurations of **CyPd** according to the different chemical connectivity.

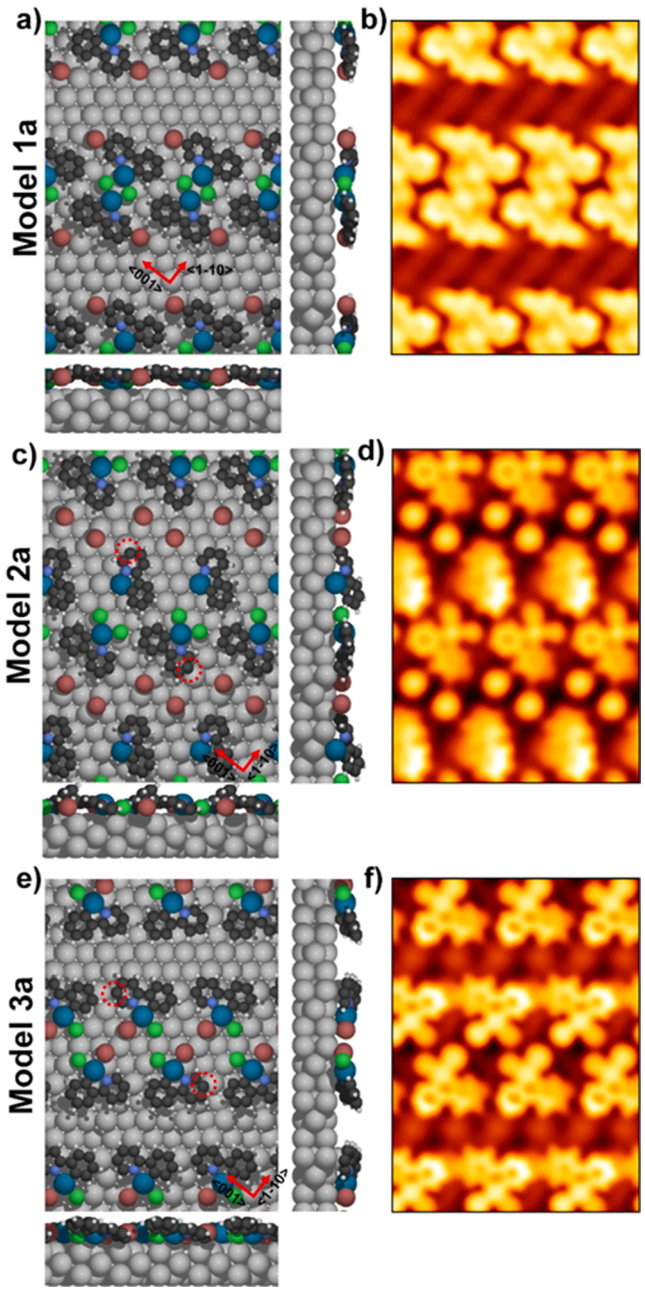

Fig. 5. Top and side view for **CyPd**/Ag(1 1 0) and simulated STM image for: a-b) Model 1a (undissociated molecule), c-d) Model 2a (dissociated molecule), and e-f) Model 3a (dissociated molecule). Red lines indicate the two main crystallographic directions: ⟨0 0 1⟩, and ⟨1–1 0⟩. Atoms color code is the same as reported in Fig. 4b. V = −0.1 V, ILDOS *iso*-surface value of 8×10^{-6} $|e|/a_0^3$. Dashed red circle indicates the undercoordinated C atoms previously bonded to Br atoms.

smaller size than the one expected for a whole molecule. Therefore, we considered the possibility that **CyPd** does not only lose the bromine atoms, which adsorb on the surface, but that it also splits in two parts (Model 2 in Fig. 4b). During the splitting, the two Cl atoms may remain attached to the same Pd atom ($C_{11}H_7NPdCl_2$ + $C_{11}H_7NPd$, Model 2a in Fig. 5c) or bind to the different Pd atoms in a symmetric dissociation mode ($C_{11}H_7NPdCl$ + $C_{11}H_7NPdCl$, Model 2b in Figure S6c). Dissociation may be favored by the interaction between the Pd atoms with the underlying Ag surface atoms. The resulting STM features are smaller, in good agreement with the experimental ones. However, the orientation of the separated fragment is different, and the Br atoms fill the external row between fragments of different molecules. The features are not as homogeneously distributed on the surface as in the experimental STM image. To improve this aspect of the model, we attached each Br atom to the Pd of a different fragment ($C_{11}H_7NPdClBr$ + $C_{11}H_7NPdClBr$, Model 3a in Fig. 5e). The resulting pattern fits the STM images better except that the bright features within the cell are facing each other, unlike in the experiment. In addition, the two rows in a pair are too close to each other, leaving too much empty space between paired rows. Therefore, we rotated (Model 3b in Fig. 6a) or shifted (Model 3c in Fig. 6c) the $C_{11}H_7NPdClBr$ fragments further apart to make a more even separation between pairing rows, but the results were still not in satisfactory agreement with the experimental image. Indeed, the two halves of the

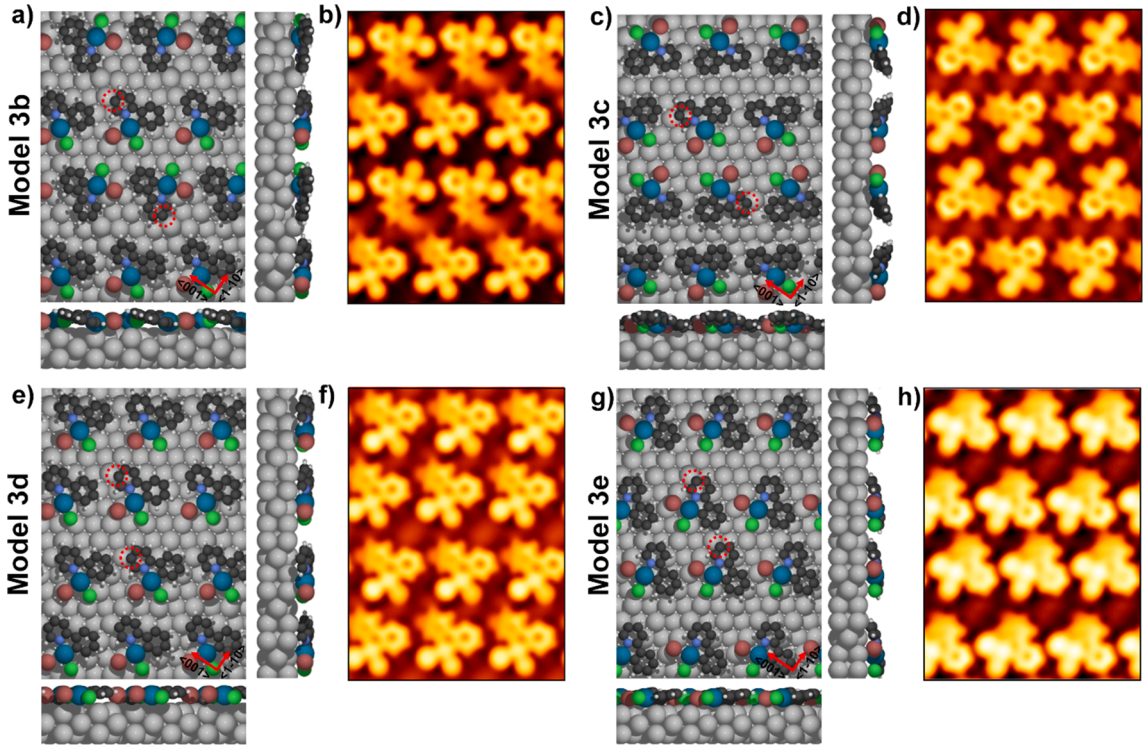

Fig. 6. Top and side view for CyPd/Ag(1 1 0) along with the simulated STM image for: a-b) Model 3b, c-d) Model 3c, e-f) Model 3d, and g-h) Model 3e. Red lines indicate the two main crystallographic directions: ⟨0 0 1⟩, and ⟨1 –1 0⟩. Atoms color code is the same as reported in Fig. 4b. V = −0.1 V, ILDOS *iso*-surface value of 8×10^{-6} $|e|/a_0^3$. Dashed red circle indicates the undercoordinated C atoms previously bonded to Br atoms.

molecule are equivalent, but they do not have the same orientation, contrary to the experimentally observed features. To achieve the homogeneous pattern of the experimental images, the molecular fragments cannot face each other as they would after dissociation. Instead, one of the two fragments in the pair must fully rotate to become essentially indistinguishable from the other. This can be obtained considering different adsorption patterns, as shown in Model 3d and Model 3e (Fig. 6e and g). The bright feature now looks more like the repeating bright entities in the experimental STM image, except for the fact that they occupy more space in the repeating unit than what was observed in the experiments; in addition, the bright spheres between the molecular fragments (two for each fragment) are missing. We believe that those spheres are dissociated Br and Cl atoms, therefore, we break the Pd-Br and Pd-Cl bonds and detach the Br and Cl atoms from the molecular fragments ($C_{11}H_7NPd/Cl/Br + C_{11}H_7NPd/Cl/Br$, Model 4 in Figure S7). This caused a tilting of the molecule since the unsaturated Pd atom migrates deeper in the Ag layer in a 4-fold hollow position. Finally, since the Pd atom was found to be screened according to XPS measurements, we have considered the possibility that the Pd atom migrates below, in the sublayers of the Ag surface being replaced by one Ag adatom from the surface through a metal exchange mechanism (Model 4-Ag in Fig. 7). The new configuration is a stable minimum (+50 meV with respect to

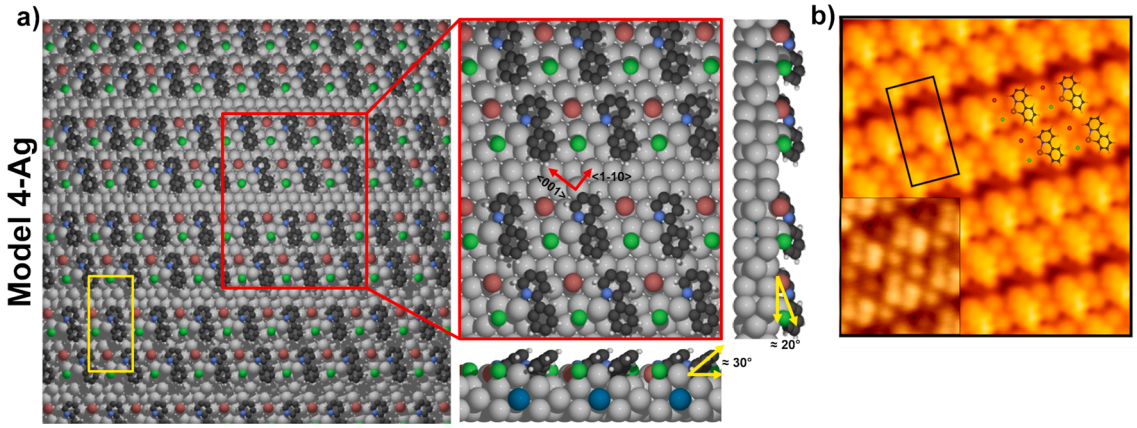

Fig. 7. a) Top and side view for Model 4-Ag of **CyPd**/Ag(1 1 0). Red lines indicate the two main crystallographic directions ⟨0 0 1⟩ and ⟨1 –1 0⟩. Yellow lines indicate the estimated tilting angle values for the molecular fragments with respect to the metal surface plane. The unit cell is indicated by a yellow box. Atoms color code is the same as reported in Fig. 4b. **b**) Simulated STM image (V = −0.5 V) with the optimized DFT adsorption configuration overlayed (Model 4-Ag). The two lozenge shaped features correspond to the phenyl-pyridine unit bridged by Ag adatom (orange ball); the fainter surrounding dots are the dissociated Br (red ball) and Cl atoms (green ball). The pyridinic part of the ring has darker contrast with respect to the phenyl ring, appearing as a brighter protrusion in the STM image. Pd occupies the octahedral sites below the surface and hence it does not appear in the figure. The corresponding experimental STM image is reported in the bottom-left corner to underline the good matching.

model 4a) and, considering the increase in the overall system disorder, it is certainly entropically more favorable. The atomic charge on the Ag atom attached to the phe-pyr fragment (+0.37 e^-) is about the same as the one calculated for the Pd atom (+0.39 e^-) in the previous model 4a (see Table S4). Therefore, Model 4-Ag is the structure that best fits the experimental findings, as it will be discussed in the next section.

To summarize, we have developed the following chemical and conformational steps, taking place on the surface upon deposition of the $C_{22}H_{14}Br_2N_2Pd_2Cl_2$ complex:

(1) Debromination:

$$C_{22}H_{14}Br_2N_2Pd_2Cl_2 \rightarrow C_{22}H_{14}N_2Pd_2Cl_2 + 2Br_{ads}$$

(2) Dissociation in two symmetric fragments.

$$C_{22}H_{14}N_2Pd_2Cl_2 \rightarrow C_{11}H_7NPdCl + C_{11}H_7NPdCl + 2Br_{ads}$$

(3) Dechlorination

$$C_{11}H_7NPdCl + C_{11}H_7NPdCl + 2Br_{ads} \rightarrow C_{11}H_7NPd + C_{11}H_7NPd + 2Br_{ads} + 2Cl_{ads}$$

(4) Rotation of fragments and tilting
(5) Metal exchange between Pd and Ag

$$C_{11}H_7NPd/Ag_{bulk} \rightarrow C_{11}H_7NAg/Pd_{bulk}$$

The order in which these steps happen on the surface is not definitively determined.

Metal ion exchange between organometallic compounds and the metallic substrate have already been reported for several systems, as Ni porphyrins [50] and Co phthalocyanines [51] on Cu(1 1 1). The exchange is favored by annealing of the adsorbed layer but, when the molecules are sublimed at 700 K, their high thermal energy ignites the process already at RT. We do not believe this holds in the present case, in which the molecules were sublimed at 130 °C (403 K). On the contrary, the exchange may be favored by the dissociation of the ***CyPd*** complex upon interaction with the Ag surface. Diffusion of the Pd atom below the surface is not surprising, since the surface energy of Pd is significantly higher than that of Ag [52] (2.05 J/m^2 for Pd and 1.25 J/$m/^2$ for Ag), so that Pd atoms tend to migrate into the bulk of the Ag crystal. This is confirmed by state-of-the-art calculations on the growth of bimetallic AgPd clusters, showing the formation of a core–shell structure with Pd atoms preferentially in subsurface sites [53].

To verify this trend, and since our XPS data suggest that Pd atoms may go deeper into the crystal, we repeated the geometry optimization of *Model 4-Ag of **CyPd**/Ag(1 1 0)* increasing the slab thickness from 3 Ag layers up to 5 and 7 Ag layers. The outcome indicates that in the most stable configuration the Pd atoms are always in the middle of the slab (i.e. in the central Ag layer), with a gain in energy of −0.06 and −0.08 eV/Pd for the 5-layer and 7-layer slabs, respectively. The segregation effect of Pd in the subsurface metal layers can be even further facilitated by the high mobility of Ag atoms at the surface, which was not taken into account in the simulations and would support the experimental information.

3.3. Discussion

To check the validity of our final adsorption model, we simulated the STM image derived from Model 4-Ag. The outcome, reported in Fig. 7b for a bias voltage V = −0.5 V, shows a good agreement with the corresponding experimental image (see bottom-left corner). The same comparison at different biases is available in the SM (Figure S8). The double row pattern, the unit cell geometry and the position of the molecular fragments (superimposed to the image to allow for a clearer assignment) are well reproduced by the simulation. The four interstitial dots present in each unit cell are assigned to the two Br adatoms in 4-fold hollow sites and to the two Cl adatoms in 3-fold hollow sites, respectively. This behavior is similar to what has been reported for other halogenated aromatic systems on the same substrate [26]. Lozenges correspond to phenyl-pyridine units coordinated to one Ag adatom. The different brightness of the lobes within the same lozenge is well reproduced by the model, which apparently suggests the pyridinic ring to be darker than the phenyl one. However, more information can be obtained from the inspection of the STS spectra and dI/dV maps reported in Fig. 8.

The STM image of panel a) is well compatible with the double row structure described in Figs. 1 and 2, though the internal structure of the lozenges is not evident due to the lower resolution. The STS spectrum of panel d) is measured at the center of a lozenge (cross in a) and shows the local density of states of CyPd around the Fermi Edge. We mention that STS measurements performed at different points of the unit cell gave spectra equivalent to the one of panel d), which is characterized by a weak state at V ∼ +0.20 V and by a broad and more intense one at V ∼ − 0.31 V. The rising tail above + 0.5 V is coherent with that observed for other aromatic compounds as benzene [54]. dI/dV maps recorded in correspondence of the observed states (panels b and c) show that the lozenges corresponding to phenyl-pyridine units have a different contrast at the two bias voltages. These differences are reflected in the line scans of panel e), cut along the lines marked on the dI/dV maps: while a lower and broader corrugation is found for V = +0.20 V, the profile measured at V = −0.31 V is sharper and with slightly asymmetric shape induced by the presence of a bright spot in each lozenge. STS and dI/dV maps suggest, therefore, the presence of a localized state around V = −0.31 V, in a position well-suited for the N atom in the pyridinic ring. This assignment agrees with the STS spectra of N-doped graphene with N atoms in pyridinic configuration [55], while the benzene ring is expected to have an empty state at higher energy (approximately 2.0 V) [54].

The NEXAFS spectra of Fig. 9 report the C and N K-edges recorded after deposition of a full monolayer of **CyPd** on Ag(1 1 0) at RT. Main resonances are present at 284.2 eV, with a shoulder at 284.8 eV and at 288.7 eV in the C K-edge spectrum recorded in p-polarization (continuous lines). Their intensity is reduced by a factor of ∼ 10 in the s-polarization spectra (dashed lines), while broad structures centered around 293 eV and 300 eV appear. The energy region below 290 eV is dominated by π* resonances. We identify the peak at 284.2 eV and the smaller one at 288.7 eV with the 1s → π_1* and 1s → π_2* transitions from C 1s occupied core-levels to the lowest unoccupied molecular levels (LUMOs), in agreement with what reported in previous literature for the aromatic systems of phenyl rings [56]. The shoulder at 284.8 eV in the main π* resonance is likely related to the non-equivalent C atoms bound to N atoms in the pyridine unit [57]. A contribution of C-Ag interaction to the NEXAFS features cannot be excluded. The energy region above 290 eV is characterized by σ* resonances.

The N K-edge spectra show peaks at 398.6 eV and 402.9 eV in p-polarization, while a large resonance around 408 eV is dominant in s-polarization. These features are assigned to the transition of N 1s electrons into the π_1*, π_3* and σ* molecular states, respectively, in good agreement with what reported for gas-phase pyridine [57] and for pyridine compounds on Au [46,58].

The strong polarization dependence of NEXAFS spectra implies a preferential orientation of the molecules. However, the residual intensity of π* transitions in the s-polarization spectra indicates that the molecular plane is not flat with respect to the surface. An estimation of the molecular tilt angle can be given by evaluating the s-/p-polarization intensity ratio and following the approach indicated by Stohr for a two-fold symmetry domain [31]. Considering the error introduced by the spectra normalization procedure as well as the azimuthal misalignment of the beam electric field with respect to the ⟨0 0 1⟩ direction due to the sample mounting, we found that the spectra describe the molecules as tilted by (20 ± 10)°. This estimate is compatible with the theoretical model (see Fig. 7a) and supports its validity.

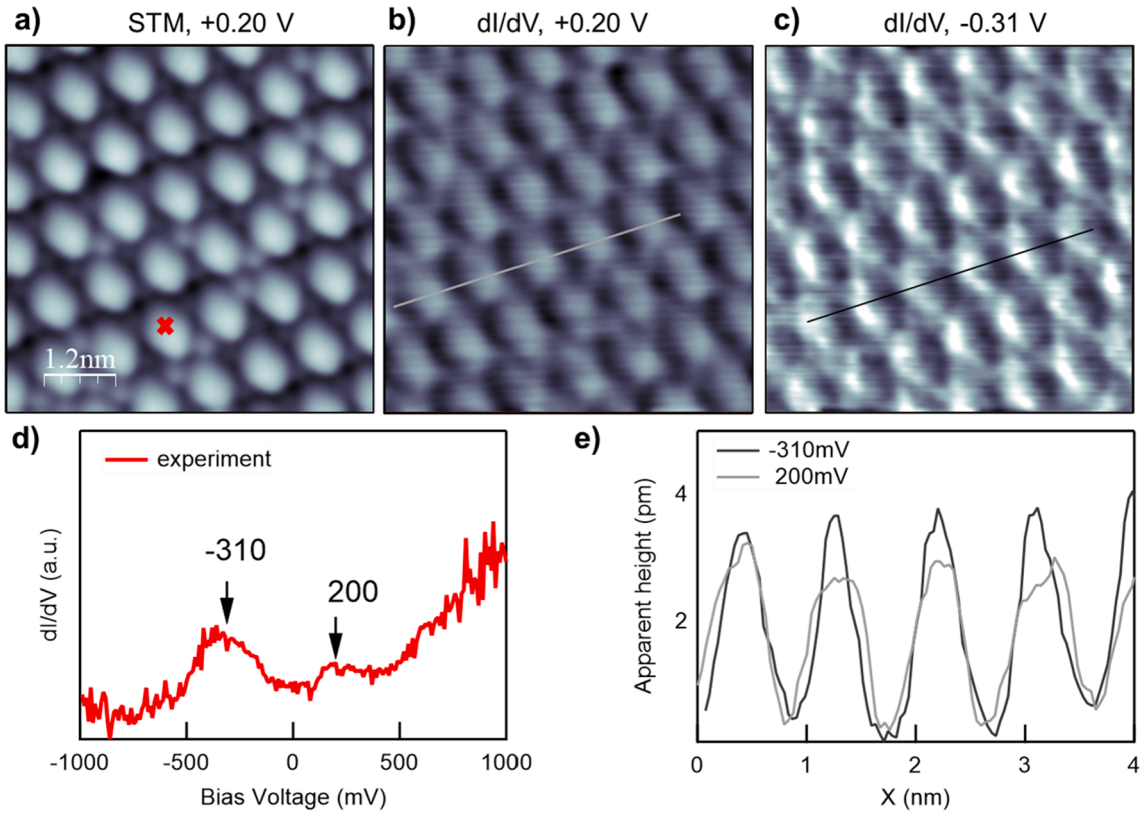

Fig. 8. **a)** STM image of **CyPd** upon RT deposition. The red cross marks the point where the STS spectrum of panel **d)** was recorded. Image size: 6.0 × 6.0 nm^2, V = +0.2 V, I = 0.42 nA. **b) and c)** dI/dV maps taken at the bias voltages corresponding to local maxima in the STS spectrum of panel **d). e)** Line scans cut along the grey and black traces marked in the **b)** and **c)**.

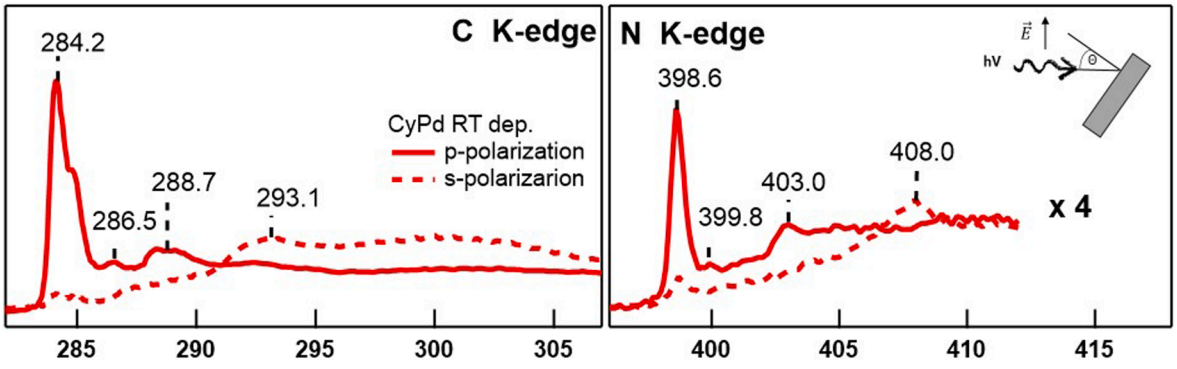

Fig. 9. NEXAFS spectra of the C K-edge and N K-edge recorded with the linearly polarized photon beam impinging normal to the surface (corresponding to s-polarization) and at 85° incidence (corresponding to p-polarization).

4. Conclusions

In this work, we present the first investigation of the self-assembly of Pd-cyclometallated compounds deposited on a noble metal surface. The **CyPd**/Ag(1 1 0) system shows an unexpected and peculiar behavior. An ordered self-assembled layer of paired rows of lozenge-shaped features with interstitial dots in between them forms. A deeper analysis and a mechanistic study, based on density functional theory calculations and corroborated by the experimental findings, indicate that the molecule dissociates due to the interaction with the metal substrate: the halogen atoms bind to the surface, the two phe-pyr fragments saturate towards an Ag adatom and the Pd atoms diffuse inside the Ag substrate. Therefore, the formation of a C-based network at the surface occurs upon a drastic modification of the system, in which metal atoms are embedded in regular positions. The atomistic details of reaction steps reveal the active role played by the metal substrate in promoting the chemistry of the deposited Pd cyclometallates. We believe that our results open new perspectives for the exploitation of this class of materials in heterogeneous catalytic applications. On one hand, metal atoms protruding from the surface and bound to the phe-pyr units should be chemically different from those in the surface and possibly exhibit a peculiar reactivity. Though out of the scope of the present manuscript, this study represents the natural evolution of the research. On the other hand, the possibility of interaction and cross-coupling between the phe-pyr fragments is under investigation [59] and can be extended to different systems by careful choice of the initial precursor molecule.

5. Associated content

The supporting information file contains the following material, referenced in the text:

- CyPd synthesis detail and characterization before and after sublimation in UHV.
- Additional experimental results.
- Intermediate DFT models and calculations non presented in the main manuscript.
- Additional comparison between experimental and simulated STM images.

Author Contributions

M.S.: Investigation, Formal analysis, Writing original draft (experimental); D.P.: Investigation, formal analysis, Writing original draft (Theoretical); J.E.B.: Investigation, Formal analysis; M.S.: Investigation (experimental - XPS); G.C.: Investigation (experimental – STM); T.H.D.: Formal analysis (XPS); L.V.: Writing – Review and Editing; M.R.: Writing – Review and Editing; G.B.: Concepualization, Writing – Review and Editing; M.D.A.: Investigation (XPS); R.C.: Investigation (XPS); A.C.: Investigation (XPS); L.V.: Investigation (Synthesis); A.P.: Investigation (Synthesis); C.D.V.: Conceptualization, Supervision, Funding acquisition (theoretical); L.S.: Conceptualization, Supervision, Project administration and Funding acquisition (experimental). All authors actively contributed to the Writing – Review and Editing process.

Declaration of Competing Interest

The authors declare that they have no known competing financial interests or personal relationships that could have appeared to influence the work reported in this paper.

Acknowledgments

We acknowledge financial support from MIUR through projects PRIN2017 n. 2017NYPHN8 and from Fondazione Compagnia di S. Paolo through project MC-nano. We acknowledge Elettra Sincrotrone Trieste for providing access to its synchrotron radiation facilities and for financial support.

Appendix A. Supplementary material

Supplementary data to this article can be found online at https://doi.org/10.1016/j.apsusc.2022.154960.

References

[1] H. Chen, Y. Li, S. Liu, Q. Xiong, R. Bai, D. Wei, Y. Lan, On the mechanism of homogeneous Pt-catalysis: A theoretical view, Coord. Chem. Rev. 437 (2021) 213863, https://doi.org/10.1016/j.ccr.2021.213863.
[2] P. Sehnal, R.J.K. Taylor, L.J.S. Fairlamb, Emergence of palladium(IV) chemistry in synthesis and catalysis, Chem. Rev. 110 (2010) 824–889, https://doi.org/10.1021/cr9003242.
[3] A. Biffis, P. Centomo, A. Del Zotto, M. Zecca, Pd Metal Catalysts for Cross-Couplings and Related Reactions in the 21st Century: A Critical Review, Chem. Rev. 118 (2018) 2249–2295, https://doi.org/10.1021/acs.chemrev.7b00443.
[4] M. Mauro, A. Aliprandi, D. Septiadi, N.S. Kehr, L. De Cola, When self-assembly meets biology: Luminescent platinum complexes for imaging applications, Chem. Soc. Rev. 43 (2014) 4144–4166, https://doi.org/10.1039/c3cs60453e.
[5] M. Fanelli, M. Formica, V. Fusi, L. Giorgi, M. Micheloni, P. Paoli, New trends in platinum and palladium complexes as antineoplastic agents, Coord. Chem. Rev. 310 (2016) 41–79, https://doi.org/10.1016/j.ccr.2015.11.004.
[6] F. De Castro, E. De Luca, M. Benedetti, F.P. Fanizzi, Platinum compounds as potential antiviral agents, Coord. Chem. Rev. 451 (2022) 214276, https://doi.org/10.1016/j.ccr.2021.214276.
[7] V.W.W. Yam, V.K.M. Au, S.Y.L. Leung, Light-Emitting Self-Assembled Materials Based on d8 and d10 Transition Metal Complexes, Chem. Rev. 115 (2015) 7589–7728, https://doi.org/10.1021/acs.chemrev.5b00074.
[8] J. Kalinowski, V. Fattori, M. Cocchi, J.A.G. Williams, Light-emitting devices based on organometallic platinum complexes as emitters, Coord. Chem. Rev. 255 (2011) 2401–2425, https://doi.org/10.1016/j.ccr.2011.01.049.
[9] D.C. Powers, T. Ritter, Palladium(III) in synthesis and catalysis, Top. Organomet. Chem. 503 (2011) 129–156, https://doi.org/10.1007/978-3-642-17429-2_6.
[10] R. Mosteiro, A. Fernández, D. Vázquez-García, M. Lõpez-Torres, A. Rodríguez-Castro, N. Gõmez-Blanco, J.M. Vila, J.J. Fernández, Cyclometallated palladium diphosphane compounds derived from the chiral ligand (S)-PhCH(Me)NMe2. Michael addition reactions to the vinylidene double bond, Eur. J. Inorg. Chem. (2011) 1824–1832, https://doi.org/10.1002/ejic.201000873.
[11] V.K. Jain, Cyclometalated group-16 compounds of palladium and platinum: Challenges and opportunities, Coord. Chem. Rev. 427 (2021) 213546, https://doi.org/10.1016/j.ccr.2020.213546.
[12] M. Albrecht, Cyclometalation using d-block transition metals: Fundamental aspects and recent trends, Chem. Rev. 110 (2010) 576–623, https://doi.org/10.1021/cr900279a.
[13] S. Wilde, D. Ma, T. Koch, A. Bakker, D. Gonzalez-Abradelo, L. Stegemann, C. G. Daniliuc, H. Fuchs, H. Gao, N.L. Doltsinis, L. Duan, C.A. Strassert, Toward Tunable Electroluminescent Devices by Correlating Function and Submolecular Structure in 3D Crystals, 2D-Confined Monolayers, and Dimers, ACS Appl. Mater. Interfaces. 10 (2018) 22460–22473, https://doi.org/10.1021/acsami.8b03528.
[14] J. Ren, M. Cnudde, D. Brünink, S. Buss, C.G. Daniliuc, L. Liu, H. Fuchs, C. A. Strassert, H.Y. Gao, N.L. Doltsinis, On-Surface Reactive Planarization of Pt(II) Complexes, Angew. Chemie - Int. Ed. 58 (2019) 15396–15400, https://doi.org/10.1002/anie.201906247.
[15] H. Gersen, R. Schaub, W. Xu, I. Stensgaard, E. Laegsgaard, T.R. Linderoth, F. Besenbacher, M.K. Nazeeruddin, M. Graetzel, Dissociation of iridium(III) phosphorescent emitters upon adsorption on Cu(110) revealed by scanning tunneling microscopy, Appl. Phys. Lett. 89 (2006) 10–13, https://doi.org/10.1063/1.2424675.
[16] C.N.R. Rao, K. Gopalakrishnan, A. Govindaraj, Synthesis, properties and applications of graphene doped with boron, nitrogen and other elements, Nano Today. 9 (2014) 324–343, https://doi.org/10.1016/j.nantod.2014.04.010.
[17] X. Yang, X. Dou, A. Rouhanipour, L. Zhi, H.J. Räder, K. Müllen, Two-dimensional graphene nanoribbons, J. Am. Chem. Soc. 130 (2008) 4216–4217, https://doi.org/10.1021/ja710234t.
[18] X. Li, X. Wang, L. Zhang, S. Lee, H. Dai, Chemically derived, ultrasmooth graphene nanoribbon semiconductors, Science (80-.). 319 (2008) 1229–1232. https://doi.org/10.1126/science.1150878.
[19] L. Jiao, L. Zhang, X. Wang, G. Diankov, H. Dai, Narrow graphene nanoribbons from carbon nanotubes, Nature. 458 (2009) 877–880, https://doi.org/10.1038/nature07919.
[20] M.Y. Han, B. Özyilmaz, Y. Zhang, P. Kim, Energy band-gap engineering of graphene nanoribbons, Phys. Rev. Lett. 98 (2007) 1–4, https://doi.org/10.1103/PhysRevLett.98.206805.
[21] X. Li, M. Gan, L. Ma, W. Zhao, Y. Zhang, L. Wang, X. Hua, Facile synthesis of N-doped carbon nanotubes grafted on N-doped carbon nanosheets co-encapsulating cobalt and molybdenum carbide nanoparticles for efficient methanol oxidation, Mater. Today Chem. 23 (2022), https://doi.org/10.1016/j.mtchem.2021.100665.
[22] J. Hu, J. Hu, Z. Zhang, K. Shen, Z. Liang, H. Zhang, Q. Tian, P. Wang, Z. Jiang, H. Huang, J.W. Wells, F. Song, Ullmann coupling of 2,7-dibromopyrene on Au(1 1 1) assisted by surface adatoms, Appl. Surf. Sci. 513 (2020), 145797, https://doi.org/10.1016/j.apsusc.2020.145797.
[23] M. Smerieri, I. Píš, L. Ferrighi, S. Nappini, A. Lusuan, C. Di Valentin, L. Vaghi, A. Papagni, M. Cattelan, S. Agnoli, E. Magnano, F. Bondino, L. Savio, Synthesis of graphene nanoribbons with a defined mixed edge-site sequence by surface assisted polymerization of (1,6)-dibromopyrene on Ag(110), Nanoscale. 8 (2016) 17843–17853, https://doi.org/10.1039/c6nr05952j.
[24] S. Lee, Y.W. Lee, D.H. Kwak, J.Y. Lee, S.B. Han, J.I. Sohn, K.W. Park, Three-dimensional porous metal–nitrogen doped carbon nanostructure as a superior non-precious electrocatalyst in oxygen reduction reaction, J. Ind. Eng. Chem. 43 (2016) 170–176, https://doi.org/10.1016/j.jiec.2016.08.004.
[25] P. Sarkar, A. Hazra Chowdhury, S. Biswas, A. Khan, S.M. Islam, 2D covalent organic framework: a photoactive heterogeneous catalyst for chemical fixation of CO2 over propargyl amines in water under sunlight, Mater. Today Chem. 21 (2021) 100509, https://doi.org/10.1016/j.mtchem.2021.100509.
[26] M. Smerieri, I. Píš, L. Ferrighi, S. Nappini, A. Lusuan, L. Vattuone, L. Vaghi, A. Papagni, E. Magnano, C. Di Valentin, F. Bondino, L. Savio, Synthesis of corrugated C-based nanostructures by Br-corannulene oligomerization, Phys. Chem. Chem. Phys. 20 (2018) 26161–26172, https://doi.org/10.1039/c8cp04791j.
[27] X. Peng, Y. Zhu, T.A. Ramirez, B. Zhao, Y. Shi, New reactivity of oxaziridine: Pd(II)-catalyzed aromatic C-H ethoxycarbonylation via C-C bond cleavage, Org. Lett. 13 (2011) 5244–5247, https://doi.org/10.1021/ol2021252.
[28] I. Horcas, R. Fernández, J.M. Gómez-Rodríguez, J. Colchero, J. Gómez-Herrero, A. M. Baro, WSXM: A software for scanning probe microscopy and a tool for nanotechnology, Rev. Sci. Instrum. 78 (2007), https://doi.org/10.1063/1.2432410.
[29] R. Costantini, M. Stredansky, D. Cvetko, G. Kladnik, A. Verdini, P. Sigalotti, F. Cilento, F. Salvador, A. De Luisa, D. Benedetti, L. Floreano, A. Morgante, A. Cossaro, M. Dell'Angela, ANCHOR-SUNDYN: A novel endstation for time resolved spectroscopy at the ALOISA beamline, J. Electron Spectros. Relat. Phenomena. 229 (2018) 7–12, https://doi.org/10.1016/j.elspec.2018.09.005.
[30] P.H. Citrin, G.K. Wertheim, Y. Baer, Surface-atom x-ray photoemission from clean metals: Cu, Ag, and Au, Phys. Rev. B. 27 (1983) 3160–3175, https://doi.org/10.1103/PhysRevB.27.3160.

[31] J. Stöhr, NEXAFS spectroscopy by Joachim Stöhr (z-lib, NEXAFS, Spectrosc. 25 (1992) 114–161, https://doi.org/10.1007/978-3-662-02853-7.
[32] P. Giannozzi, S. Baroni, N. Bonini, M. Calandra, R. Car, C. Cavazzoni, D. Ceresoli, G.L. Chiarotti, M. Cococcioni, I. Dabo, A. Dal Corso, S. De Gironcoli, S. Fabris, G. Fratesi, R. Gebauer, U. Gerstmann, C. Gougoussis, A. Kokalj, M. Lazzeri, L. Martin-Samos, N. Marzari, F. Mauri, R. Mazzarello, S. Paolini, A. Pasquarello, L. Paulatto, C. Sbraccia, S. Scandolo, G. Sclauzero, A.P. Seitsonen, A. Smogunov, P. Umari, R.M. Wentzcovitch, QUANTUM ESPRESSO: A modular and open-source software project for quantum simulations of materials, J. Phys. Condens. Matter. 21 (2009), https://doi.org/10.1088/0953-8984/21/39/395502.
[33] P. Giannozzi, O. Baseggio, P. Bonfà, D. Brunato, R. Car, I. Carnimeo, C. Cavazzoni, S. De Gironcoli, P. Delugas, F. Ferrari Ruffino, A. Ferretti, N. Marzari, I. Timrov, A. Urru, S. Baroni, Quantum ESPRESSO toward the exascale, J. Chem. Phys. 152 (2020), https://doi.org/10.1063/5.0005082.
[34] P. Giannozzi, O. Andreussi, T. Brumme, O. Bunau, M.B. Nardelli, M. Calandra, R. Car, C. Cavazzoni, D. Ceresoli, M. Cococcioni, et al., Advanced capabilities for materials modelling with Quantum ESPRESSO. (arXiv:1709.10010v1 [cond-mat.mtrl-sci]), J. Phys. Condens. Matter. 29 (2017) 465901.
[35] K. Lee, É.D. Murray, L. Kong, B.I. Lundqvist, D.C. Langreth, Higher-accuracy van der Waals density functional, Phys. Rev. B - Condens. Matter Mater. Phys. 82 (2010), https://doi.org/10.1103/PhysRevB.82.081101.
[36] I. Hamada, M. Otani, Comparative van der Waals density-functional study of graphene on metal surfaces, Phys. Rev. B - Condens. Matter Mater. Phys. 82 (2010) 1–4, https://doi.org/10.1103/PhysRevB.82.153412.
[37] I. Píš, L. Ferrighi, T.H. Nguyen, S. Nappini, L. Vaghi, A. Basagni, E. Magnano, A. Papagni, F. Sedona, C. Di Valentin, S. Agnoli, F. Bondino, Surface-Confined Polymerization of Halogenated Polyacenes: The Case of Dibromotetracene on Ag (110), J. Phys. Chem. C. 120 (2016) 4909–4918, https://doi.org/10.1021/acs.jpcc.5b12047.
[38] L. Ferrighi, I. Píš, T.H. Nguyen, M. Cattelan, S. Nappini, A. Basagni, M. Parravicini, A. Papagni, F. Sedona, E. Magnano, F. Bondino, C. Di Valentin, S. Agnoli, Control of the intermolecular coupling of dibromotetracene on Cu(110) by the sequential activation of C-Br and C-H bonds, Chem. - A Eur. J. 21 (2015) 5826–5834, https://doi.org/10.1002/chem.201405817.
[39] A. Basagni, L. Ferrighi, M. Cattelan, L. Nicolas, K. Handrup, L. Vaghi, A. Papagni, F. Sedona, C. Di Valentin, S. Agnoli, M. Sambi, On-surface photo-dissociation of C-Br bonds: Towards room temperature Ullmann coupling, Chem. Commun. 51 (2015) 12593–12596, https://doi.org/10.1039/c5cc04317d.
[40] J.D.P. Hendrik, J. Monkhorst, Special points for Brillonin-zone integrations*, Phys. Rev. B. 13 (1976) 5188–5192, https://doi.org/10.1103/physrevb.13.5188.
[41] D.R. Tersoff, J. Hamann, Theory of the scanning tunneling microscope, Phys. Rev. B. 31 (1985) 805–813, https://doi.org/10.1103/PhysRevB.31.805.
[42] D. Nečas, P. Klapetek, Gwyddion: An open-source software for SPM data analysis, Cent. Eur. J. Phys. 10 (2012) 181–188, https://doi.org/10.2478/s11534-011-0096-2.
[43] J. Eichhorn, D. Nieckarz, O. Ochs, D. Samanta, M. Schmittel, P.J. Szabelski, M. Lackinger, On-surface ullmann coupling: The influence of kinetic reaction parameters on the morphology and quality of covalent networks, ACS Nano. 8 (2014) 7880–7889, https://doi.org/10.1021/nn501567p.
[44] R. Gutzler, L. Cardenas, J. Lipton-Duffin, M. El Garah, L.E. Dinca, C.E. Szakacs, C. Fu, M. Gallagher, M. Vondráček, M. Rybachuk, D.F. Perepichka, F. Rosei, Ullmann-type coupling of brominated tetrathienoanthracene on copper and silver, Nanoscale. 6 (2014) 2660–2668, https://doi.org/10.1039/c3nr05710k.
[45] G.M. National Institute of Standards and Technology, NIST X-ray Photoelectron Spectroscopy Database, (2000). https://doi.org/doi:10.18434/T4T88K.
[46] Y. Zubavichus, M. Zharnikov, Y. Yang, O. Fuchs, E. Umbach, C. Heske, A. Ulman, M. Grunze, X-ray photoelectron spectroscopy and near-edge X-ray absorption fine structure study of water adsorption on pyridine-terminated thiolate self-assembled monolayers, Langmuir. 20 (2004) 11022–11029, https://doi.org/10.1021/la047980b.
[47] F. Orlando, P. Lacovig, M. Dalmiglio, A. Baraldi, R. Larciprete, S. Lizzit, Synthesis of nitrogen-doped epitaxial graphene via plasma-assisted method: Role of the graphene-substrate interaction, Surf. Sci. 643 (2016) 214–221, https://doi.org/10.1016/j.susc.2015.06.017.
[48] R.H. Temperton, A.J. Gibson, K. Handrup, J.N. O'Shea, Adsorption and charge transfer interactions of bi-isonicotinic acid on Ag(111), J. Chem. Phys. 147 (2017), https://doi.org/10.1063/1.4996746.
[49] R. Costantini, H. Ustunel, Z. Feng, M. Stredansky, D. Toffoli, G. Fronzoni, C. Dri, G. Comelli, D. Cvetko, G. Kladnik, G. Bavdek, L. Floreano, A. Morgante, A. Cossaro, Methylamine terminated molecules on Ni(1 1 1): A path to low temperature synthesis of nitrogen-doped graphene, FlatChem. 24 (2020) 100205, https://doi.org/10.1016/j.flatc.2020.100205.
[50] C.M. Doyle, J.P. Cunniffe, S.A. Krasnikov, A.B. Preobrajenski, Z. Li, N.N. Sergeeva, M.O. Senge, A.A. Cafolla, Ni-Cu ion exchange observed for Ni(II)-porphyrins on Cu (111), Chem. Commun. 50 (2014) 3447–3449, https://doi.org/10.1039/c3cc48913b.
[51] K. Shen, B. Narsu, G. Ji, H. Sun, J. Hu, Z. Liang, X. Gao, H. Li, Z. Li, B. Song, Z. Jiang, H. Huang, J.W. Wells, F. Song, On-surface manipulation of atom substitution between cobalt phthalocyanine and the Cu(111) substrate, RSC Adv. 7 (2017) 13827–13835, https://doi.org/10.1039/c7ra00636e.
[52] F.R. de Boer, R. Boom, W.C.M. Mattens, A.R. Miedema, A.K. Niessen, Cohesion in Metals, Amsterdam, 1988.
[53] F. Baletto, C. Mottet, R. Ferrando, Growth of Three-Shell Onionlike Bimetallic Nanoparticles, Phys. Rev. Lett. 90 (2003) 4, https://doi.org/10.1103/PhysRevLett.90.135504.
[54] W. Xiaoyong, G. Zijian, Targeting and delivery of platinum-based anticancer drugs, Chem. Soc. Rev. 42 (2013) 202–224, https://doi.org/10.1039/c2cs35259a.
[55] M. Inagaki, M. Toyoda, Y. Soneda, T. Morishita, Nitrogen-doped carbon materials, Carbon N. Y. 132 (2018) 104–140, https://doi.org/10.1016/j.carbon.2018.02.024.
[56] M. Di Giovannantonio, M. El Garah, J. Lipton-Duffin, V. Meunier, L. Cardenas, Y. Fagot Revurat, A. Cossaro, A. Verdini, D.F. Perepichka, F. Rosei, G. Contini, Insight into organometallic intermediate and its evolution to covalent bonding in surface-confined ullmann polymerization, ACS Nano. 7 (2013) 8190–8198, https://doi.org/10.1021/nn4035684.
[57] C. Kolczewski, R. Püttner, O. Plashkevych, H. Ågren, V. Staemmler, M. Martins, G. Snell, A.S. Schlachter, M. Sant'Anna, G. Kaindl, L.G.M. Pettersson, Detailed study of pyridine at the C 1s and N 1s ionization thresholds: The influence of the vibrational fine structure, J. Chem. Phys. 115 (2001) 6426–6437, https://doi.org/10.1063/1.1397797.
[58] O. Adak, G. Kladnik, G. Bavdek, A. Cossaro, A. Morgante, D. Cvetko, L. Venkataraman, Ultrafast Bidirectional Charge Transport and Electron Decoherence at Molecule/Surface Interfaces: A Comparison of Gold, Graphene, and Graphene Nanoribbon Surfaces, Nano Lett. 15 (2015) 8316–8321, https://doi.org/10.1021/acs.nanolett.5b03962.
[59] J.E. Barcelon, M. Stojkovska, D. Perilli, G. Carraro, M. Smerieri, L. Vattuone, M. Rocca, G. Bracco, M. Dell'Angela, R. Costantini, A. Cossaro, L. Vaghi, A. Papagni, C. Di Valentin, L. Savio, Formation of diphenyl-bipyridine units by surface assisted cross coupling in Pd-cyclometalled complexes, under revision (2022).